TECHNICAL PAPER

Analysis of propagation characteristics of AlN/diamond/Si layered SAW resonator

Luyao Wang[1] · Hongliang Wang[1]

Abstract

Surface acoustic wave (SAW) devices have attracted much attention in the field of mobile communication, such as filters and duplexers. With the upgrading of mobile networks, the requirements for the working frequency of SAW devices are gradually increasing. Traditional single-layer piezoelectric SAW devices can not meet the requirements of today's performance. However, a new type of layered structure not only meets various performance requirements, but also provides a new direction for the development of SAW devices. In this paper, a layered structure of AlN/diamond/Si SAW resonator is designed. A two-dimensional unit structure model is established. Modal analysis and admittance characteristic analysis are carried out. The optimal design structure is obtained by choosing form the thickness of different electrodes and piezoelectric layers. Following this, the transient analysis of the two-dimensional complete resonator structure is carried out. Next, the propagation characteristics are obtained, and finally the input and output signals are compared. Compared with the single piezoelectric layer structure, the phase velocity and electromechanical coupling coefficient are increased by 32.2% and 49.6% respectively. The work in this paper lays a good foundation for the fabrication of high frequency layered SAW resonators above GHz.

1 Introduction

Surface acoustic wave (SAW) device is a kind of micromechanical electronic component which can be used for signal processing. It was originally used as TV IF filter, now SAW device has been widely used in wireless communication system (Hagelauer et al. 2018), radio frequency filter (Ruppel 2017), RF tag (Sorokin and Shepeta 2017), sensors for biomolecules (Fu et al. 2017; Ritter et al. 2017) chemical (Adnan et al. 2017) and gas (Vivek and Nemade 2018). In mobile communication applications, it is because of the small size, low power loss, stable frequency characteristics, and high enough Q value of SAW devices that make their application in radio frequency terminal particularly significant (Ruppel 2017). With the development of

mobile network, higher requirements have been put forward for SAW devices, such as higher operating frequencies above GHz and higher electromechanical coupling coefficients.

The working frequency of SAW devices is mainly affected by two factors, the velocity of material and the finger width of interdigital structure. In order to improve the working frequency of SAW devices, the main research direction is to increase the phase velocity or reduce the finger width of interdigital transducer (IDT) (Fu et al. 2018). Reducing the width of the interdigital structure mainly depends on the improvement of lithography accuracy, but it will increase the difficulty of the process and be limited by the photolithography limitation (Ro et al. 2010). Large-scale fabrication is difficult to realize, so the way to achieve high frequency beyond gigahertz is usually achieved by increasing the speed of SAW. The phase velocity of surface acoustic wave (SAW) is inspired by mechanical deformation of piezoelectric materials under the excitation of alternating electric field. The phase velocity of different piezoelectric materials is different. In order to improve the phase velocity of surface acoustic wave (SAW) to meet the requirement of working frequency, one method is to apply $LiNbO_3$, $LiTaO_3$, AlN and

✉ Luyao Wang
  wlynuc@163.com

  Hongliang Wang
  wanghongliang@nuc.edu.cn

[1] National Key Laboratory for Electronic Measurement Technology, Key Laboratory of Instrumentation Science and Dynamic Measurement, Ministry of Education, North University of China, Taiyuan 030051, China

other doped piezoelectric materials to SAW device design. However, this method can not greatly increase the phase velocity. The emergence of a new layered structure solves this problem. The phase velocity and electromechanical coupling coefficient of SAW can be improved simultaneously by depositing a layer or layers of piezoelectric thin films on the surface of high-speed substrate material. Moreover, by choosing materials with different characteristics the multi-layer structures can make full use of their advantages. The functions of SAW devices can be enhanced and expanded, and their operation stability and adaptation to the working environment can also be improved. Therefore, multi-layer SAW structure is an inevitable trend for the development of high frequency and high performance SAW devices.

In recent years, multi-layer SAW devices have been studied extensively. Natalya (Natalya 2018) analyzed the high quality factor characteristics of SAW resonators with LiTaO$_3$ layered structures of different material, and compared the phase velocity and electromechanical coupling coefficient. Malik et al. (2016) gave a way about how to calculate SAW phase velocity and electromechanical coupling coefficient of AlN/SiO$_2$/Si structure, and pointed out that the thickness of piezoelectric layer in multi-layer structure has an effect on phase velocity. Luo et al. (2017) carried out a 3D modeling of ZnO/SiO$_2$/Si layered structure, and gave dispersion characteristics analysis of SH-SAW. Ro et al. (2013) studied the propagation characteristics of SAW in ZnO/AlN/diamond structure. It was found that the electromechanical coupling coefficient of the second-order modes (Sezawa modes) of SAW in ZnO/AlN/diamond structure with different thickness was the largest, up to 6.05%. Rohi et al. (2010) carried out finite element analysis (FEM) on modeling of IDT/AlN/diamond structure for IDT with different locations. The effects of different electrode materials and thickness on phase velocity, electromechanical coupling coefficient and reflectivity were given. Rodriguez-Madrid et al. (2012) designed a high frequency SAW resonator based on AlN/diamond structure. The interdigital spacing was 200 nm, the center frequency was 10–14 GHz, and the out-of-band suppression was less than 36 dB.

In specific applications, Qorvo has designed SAW dual transmitter, GPS SAW filter and L-band RF filter with working frequency of 1280 MHz. Murata manufactured RF and IF filters and duplexers operating at 1280 MHz, which are used in automotive, medical and communications fields.

In this paper, a SAW resonator with AlN/diamond/Si layered structure is designed and analyzed by finite element method. Firstly, the basic unit structure is modeled in 2D, and its modal characteristics and admittance characteristics are obtained. On this basis, piezoelectric layer thickness and electrode thickness are optimized. Finally, a complete 2D resonator structure at the target operating frequency is designed, and its transient analysis is carried out to obtain its transmission characteristics and input and output signal characteristics.

2 Principle of layered structure

The main reason why surface acoustic wave (SAW) devices with multilayer structures have been widely studied is that SAW in multilayer structures has other properties besides the characteristics of SAW in piezoelectric media (Lirong et al. 2009): the phase velocity of SAW in multilayer structure is not only related to the propagation direction, but also to the thickness of each layer, the frequency of the excitation voltage, the metallization of the surface and interface. The performance of the device can be adjusted by adjusting the thickness of the film, the type of the substrate and the shape of the electrode; because its velocity is related to frequency, SAW in multi-layer structure is dispersive wave. The phase velocity of SAW in multi-layer structure tend to be relatively high makes it easy to make devices working at tens of gigahertzs (Lei et al. 2017); there are many modes of SAW in multi-layer structures, and the best mode of SAW can be selected through analysis.

Since diamond has the fastest phase velocity among all the other materials that has been previously used due to the highest Young's modulus, high frequency SAW devices based on diamond have become one of the research focuses (Mortet et al. 2008; Sorokin et al. 2017; Burkov et al. 2018). Diamond is the most ideal substrate for high frequency SAW devices, because of its lack of piezoelectric properties, it is necessary to add a layer of piezoelectric thin film. AlN thin film is widely used, because of its high electromechanical coupling coefficient and good stability (Zhou et al. 2015; Aissa et al. 2015) comparing with other piezoelectric thin films. In addition, diamond films grown on silicon substrates have high crystalline quality, so they have been used in commercial applications and various micro-electromechanical devices. Si has considerable cost-effectiveness and mature micro-machining technology, which makes SAW layered structure based on Si substrate compatible with various mechanical structures (Naumenko 2019).

3 Design of layered structures

According to literature (Fu et al. 2018), when $a/\lambda = 0.25$, the reflectivity of the reflecting grating is the largest, that is, the metallization rate (a/p) is 0.5. The working

frequency f of SAWR designed in this paper is 1300 MHz. According to the v of the layered structure in Ref. (Nikolaou et al. 2016), here the value is 7800 m/s. According to the formula:

$$v = \lambda f. \tag{1}$$

The available wavelength is 6 μm, the metal interdigital is Al, and the interdigital period $p = \lambda/2$. The electrode width a and the electrode spacing d are equal. According to the relationship of dispersion curve in (Mortet et al. 2002) and the selection of phase velocity mentioned above, the SAW in AlN/diamond structure is mode 1, and the relative thickness kh_{AlN} of piezoelectric layer is about 1.6, where $k = 2\pi/\lambda$. Therefore, the thickness of piezoelectric layer AlN is determined to be $h1$. Since the downward energy of SAW is mainly concentrated in 1–2 wavelengths (Tang et al. 2004), the thickness of high-speed layer is $h2$ and the thickness of silicon substrate is $h3$, which can also be determined. The thickness of aluminum electrode is $h4$. According to the above design principles, the unit structure shown in Fig. 1 is obtained. The specific parameters involved are shown in Table 1.

Figure 2 is a complete two-port SAW resonator with input IDT on the left and output IDT on the right. The alternating voltage is applied at the input end and the output signal is detected at the output end. The grating structure on both sides is reflective grating, which can reduce energy lossand enhance resonance. The number of reflective gratings (RG) is the same. The spacing between IDT and reflective gratings is L_R, the spacing between IDT and reflective gratings is L_D, the output fork index is N_D, and the number of reflecting gratings is N_R.
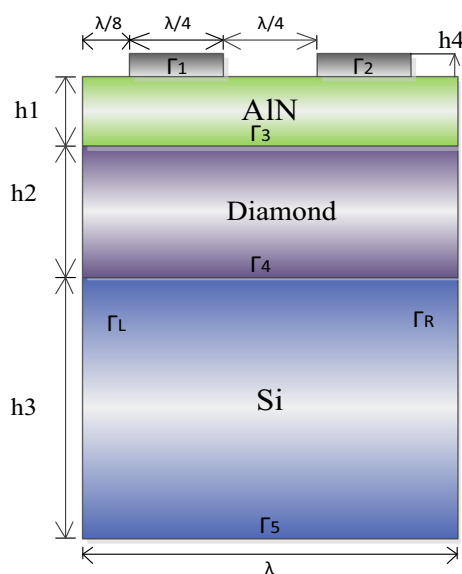

Fig. 1 IDT cell structure

4 Modeling and simulation

In this paper, COMSOL 5.3 is used to simulate and analyze the structure. In COMSOL, the coupling between structure domain and electrical domain can be expressed as the relationship between material stress and dielectric constant under constant stress, or the coupling between material strain and dielectric constant under constant strain. Generally, there are two kinds of equations: strain charge type and stress charge type.

Quasi-static equations for piezoelectric device modeling include Newton's law, Gauss's law and structural equation. The propagation of SAW can be described by differential equations, which must be solved together with design problems, including device complexity, material performance and boundary conditions. The finite element method provides the numerical solution of the definition of the related differential equation. The stress (T), strain (S), electric field (E) and electric displacement (D) of piezoelectric materials are given by the following formula (Nikolaou et al. 2016):

$$T_{ij} = c_{ijkl}^E S_{kl} - e_{kij}E_k, \tag{2}$$

$$D_i = e_{ikl}S_{kl} + \varepsilon_{ij}^S E_k, \tag{3}$$

where T_{ij} is the stress vector, c_{ijkl}^E is the elastic matrix (N/m²), e_{ikl} is the piezoelectric matrix (C/m²), ε_{ij} is the dielectric constant matrix (F/m), E_k is the displacement vector (V/m), S_{kl} is the strain vector, and D_i is the electric displacement (C/m²). Potential V can be obtained by solving Newton equation and Maxwell equation:

$$\rho \frac{\partial^2 u_i}{\partial t^2} = C_{ijkl} \frac{\partial^2 u_l}{\partial x_j \partial x_l} + e_{kij} \frac{\partial^2 \phi}{\partial x_j \partial x_l}, \tag{4}$$

$$e_{ijl} \frac{\partial^2 u_l}{\partial x_j \partial x_l} - \varepsilon_{jk} \frac{\partial^2 \phi}{\partial x_j \partial x_l} = 0, \tag{5}$$

where i, j, k = 1,2 and 3.

The material parameters involved in the finite element analysis are shown in Table 2 and the boundary conditions of the model are shown in Table 3.

4.1 Modal analysis

When Rayleigh wave propagates on the surface of piezoelectric substrates, the amplitude decreases exponentially with the depth of the substrates, and most of the energy is concentrated near the surface of the substrates. The displacement has surface normal component and surface parallel component in the direction of wave propagation, and there is no wave propagation in the parallel lateral direction. These characteristics enable us to model 2D SAWR in the case of thin piezoelectric substrates. The

Table 1 Geometric parameters for design

Unit element	$\lambda(\mu m)$	$p(\mu m)$	a/p	$h1(\mu m)$	$h2(\mu m)$	$h3(\mu m)$	$h4(\mu m)$
	6	3	1.5	1.5	3	6	0.15
SAWR	$\lambda(\mu m)$	$L_R(\mu m)$	$L_D(\mu m)$	N_D	N_R	$f(MHz)$
	6	1.5	3	8	4	1300
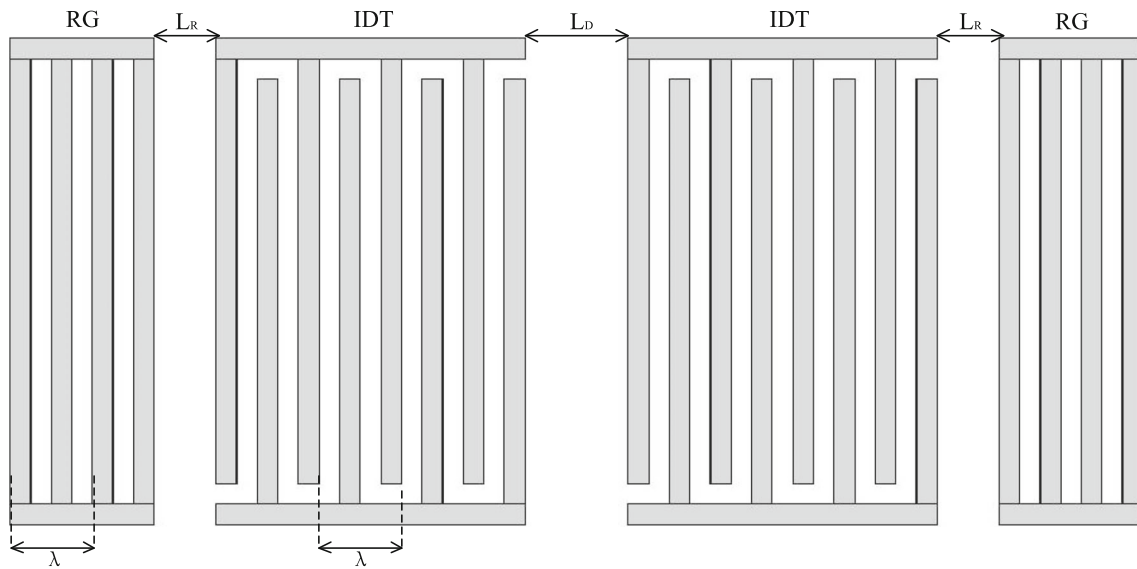
Fig. 2 Top view of two-port SAW resonator

Table 2 Material characteristic parameters for simulation

	Symbol	AlN (Maouhoub et al. 2016)	Diamond (Maouhoub et al. 2016)	Si (Aslam et al. 2018)
Density	ρ	3260	3515	2329
Elasticity matrix (GPa)	c_{11}	34.5	115.8	16.6
	c_{12}	12.5	8.5	6.39
	c_{13}	12	–	6.39
	c_{33}	39.5	–	1.66
	c_{44}	11.8	53.7	7.95
Piezoelectric constant(C/m^2)	e_{15}	− 0.48	− 0.45	–
	e_{31}	− 0.58	− 0.51	–
	e_{33}	1.5	1.22	–
Dielectric constant(10^{-11} F/m)	ε_{11}	8	7.41	11.8
	ε_{33}	9.5	7.82	11.8

periodic condition can be used to analyze multi-IDT finger pairs to establish the unit structure model (Tao et al. 2015). The eigenmode response of the element structure is obtained by eigenmode analysis as shown in Fig. 3. Then the displacement distributions of symmetric and antisymmetric modes are obtained as shown in Fig. 4. The admittance characteristics shown in Fig. 5 can obtain the electromechanical coupling coefficient, which can be calculated by the following formula (Kaletta et al. 2013):

$$K^2 = \frac{\pi^2}{4} \frac{(f_a - f_s)}{f_a}, \tag{6}$$

where f_a is an antisymmetric resonant frequency and f_s is a symmetric resonant frequency. This formula is applied to the electromechanical coupling calculation afterwards.

Table 3 Boundary conditions for simulation

	mechanical boundary conditions	Electrical boundary conditions
Γ_1, Γ_2	Free boundary	Potential/grounding
Γ_3	Free boundary	Continuity
Γ_4	Free boundary	Continuity
Γ_5	Fixed constraint	Grounding
Γ_L, Γ_R	Periodic conditions	

(a) Symmetric mode 1266.2MHz

(b) Antisymmetric mode 1273.6MHz

Fig. 3 Modal characteristics of unit structure

(a) Total displacement of symmetric modal surface
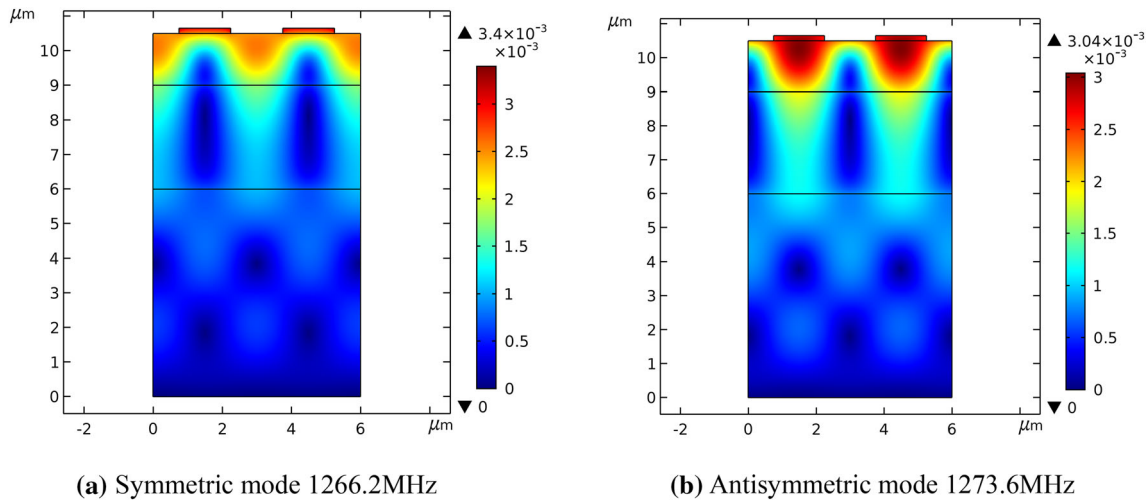
(b) Total displacement of antisymmetric modal surface
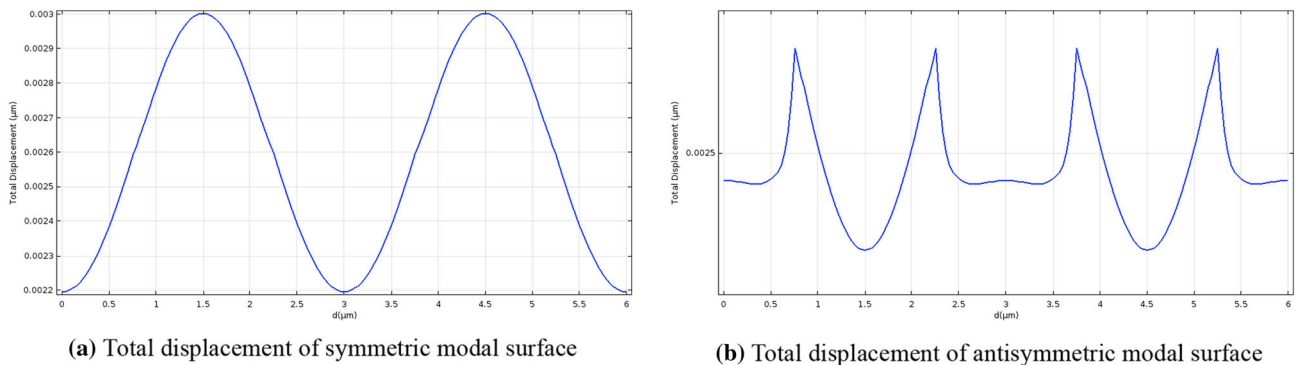
Fig. 4 Modal displacement analysis of unit structure

4.2 Geometric parameter optimization

In order to determine the optimal SAW resonator structure, the thickness of interdigital electrode and piezoelectric layer are optimized and analyzed. Considering the mass loading effect of metal electrodes (Chen et al. 2019), the resonance frequency of metal electrodes with different thicknesses is analyzed, and the optimal thickness of interdigital electrodes is obtained. The simulation results are shown in Fig. 6. Then, in order to determine the height of the piezoelectric layer, the resonant displacements of different proportions of $h1/a$ are compared, as shown in Fig. 8. By comparing the effects of different parameter structures on the electromechanical coupling coefficient, the admittance effects of electrodes and piezoelectric layers with different thickness are analyzed, as shown in Figs. 7 and 9 respectively. Tables 4 and 5 reveal the corresponding electromechanical coupling coefficients. After the above parameters are determined, the two-dimensional complete structure of SAW resonator is simulated instantaneously, then the propagation characteristics of SAW resonator are obtained, and the voltage signals on the input interdigital are compared, finally the displacement changes of the output X direction and Y direction are analyzed.
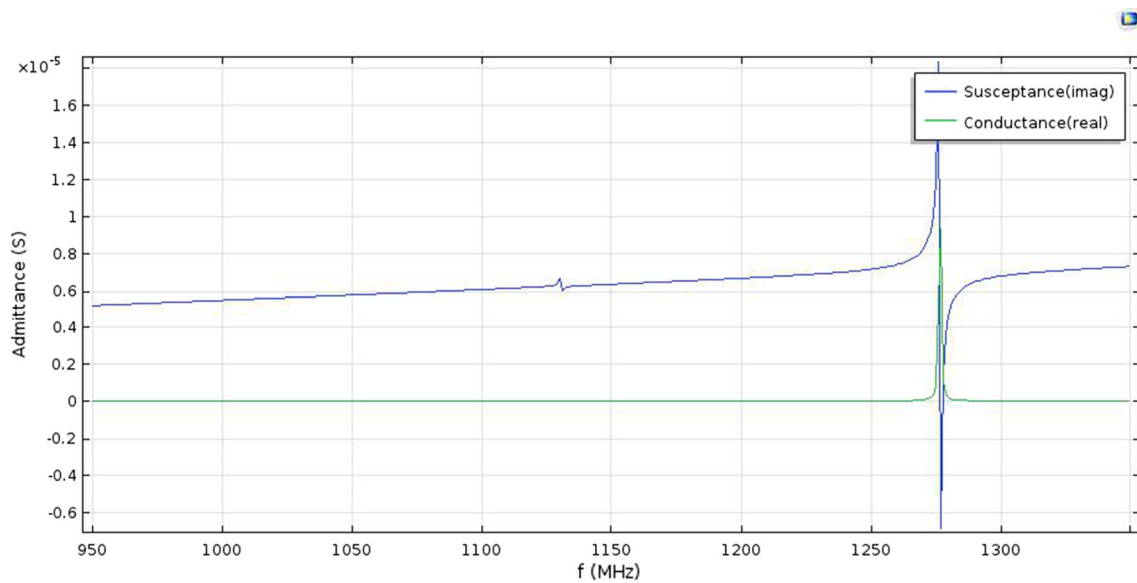
Fig. 5 Admittance characteristics of unit structure

5 Analysis of simulation results

The finite element analysis of unit structure and complete structure of Al/AlN/diamond/Si layered structure is carried out. Firstly, the characteristic frequencies of 2D structures are analyzed, as shown in Fig. 3. The resonant frequency is 1266.2 MHz, which is slightly lower than the design target. This is due to the influence of bulk wave and propagation loss. According to formula (1), the sound velocity at this time is 7591.2 m/s, which is consistent with the results given in (Mortet et al. 2008). It is higher than that of AlN film [about 5640 m/s (Ro et al. 2013)], and lower than that

of ideal diamond [about 1100 m/s (Maouhoub et al. 2016)]. The total displacement (TD) is:

$$TD = \sqrt{u^2 + v^2}, \tag{7}$$

where includes longitudinal polarization u and shear horizontal polarization v, which represent the surface displacement forms of symmetric and antisymmetric modes of the unit structure. From the admittance characteristics of Fig. 3, we can also compare the resonance peak with the anti-resonance peak and the corresponding frequency with the characteristic frequency. There is a small fluctuation at 1130 MHz, which can be caused by bulk wave interference.
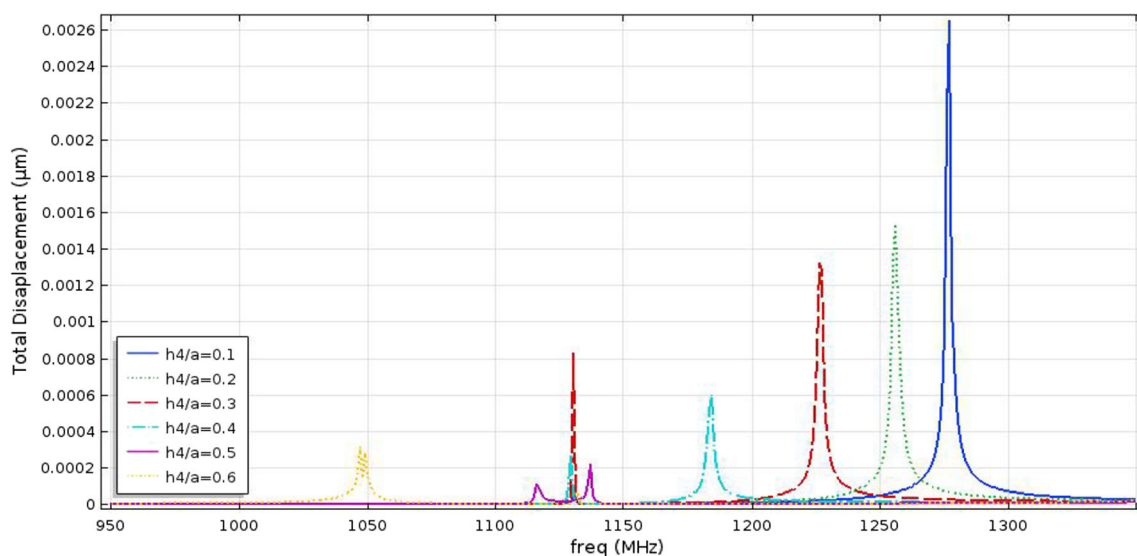

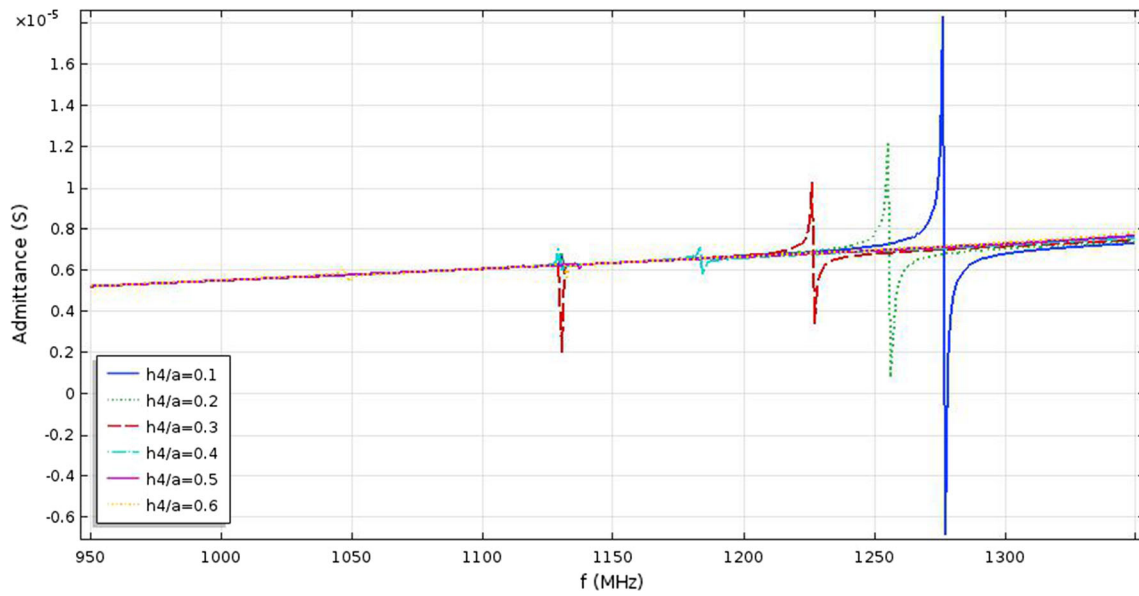**Fig. 6** The influence of interdigital thickness on resonant displacement

Fig. 7 The influence of interdigital thickness on admittance

Table 4 Effect of interdigital thickness on electromechanical coupling coefficient

$H1/a$	0.1	0.2	0.3	0.4	0.5	0.6
f_a (MHz)	1274	1261	1227	1184	1137	1049
f_s (MHz)	1266	1255	1222	1180	1134	1047
k^2 (%)	1.549	1.174	1.005	0.834	0.651	0.470

Figure 6 provides the simulation results of frequency characteristics of different interdigital thickness ratios h4/a. With the increase of metal electrode thickness, the resonance frequency decays and the displacement amplitude decreases. They are caused by the mass loading effect of metal electrode. The interference resonance appears at h4/a = 0.3. Then, the interference resonance almost overlaps the intrinsic resonance at h4/a = 0.6. Hence, it can be seen that the influence of the increase of electrode thickness on the intrinsic resonance is more obvious.

Figure 7 demonstrates the effect of different interdigital thicknesses on the admittance characteristics. It is seen that the figure that the tiny disturbance of the admittance characteristics occurs when h4/a = 0.3., which is consistent with the results in Fig. 6. With the increase of the electrode thickness, the admittance characteristics become weaker and weaker. When h4/a = 0.6, the admittance characteristic corresponding to the resonant frequency and the anti-

resonant frequency has been attenuated by an order of magnitude. Compared with the computer electric coupling coefficient in Table 4, the optimum electrode thickness can be determined as h4/a = 0.1.

Piezoelectric layer plays an important role in the propagation of SAW, and its thickness is also significant. In order to get the optimal thickness of AlN layer, the influence of different thickness on resonant frequency is analyzed and shows as Fig. 8. From the figure, it can be seen that from h1/a = 0.5 to h1/a = 0.9, the resonant displacement increases continuously, reaching the peak value when h1/a = 0.9.The resonant displacement is close to the peak at h1/a = 1.0. When the piezoelectric layer is thin, that is h1/a = 0.1, the piezoelectric layer is too thin to the non-piezoelectric layer at this time, hence the piezoelectric effect is weak. Figure 9 shows the effect of piezoelectric layer on admittance based on the analysis of resonant frequency intensity. The change of admittance characteristic intensity in the figure is basically consistent with that in Fig. 8.

Table 5 gives the electromechanical coupling coefficients calculated at the corresponding resonant and anti-resonant frequencies. It can be concluded that when h1/a = 1.0 the electromechanical coupling coefficients are 1.55%, which is 0.21% higher than when h1/a = 0.9, while the electromechanical coupling coefficients of piezoelectric

Table 5 Effect of piezoelectric layer thickness on electromechanical coupling coefficient

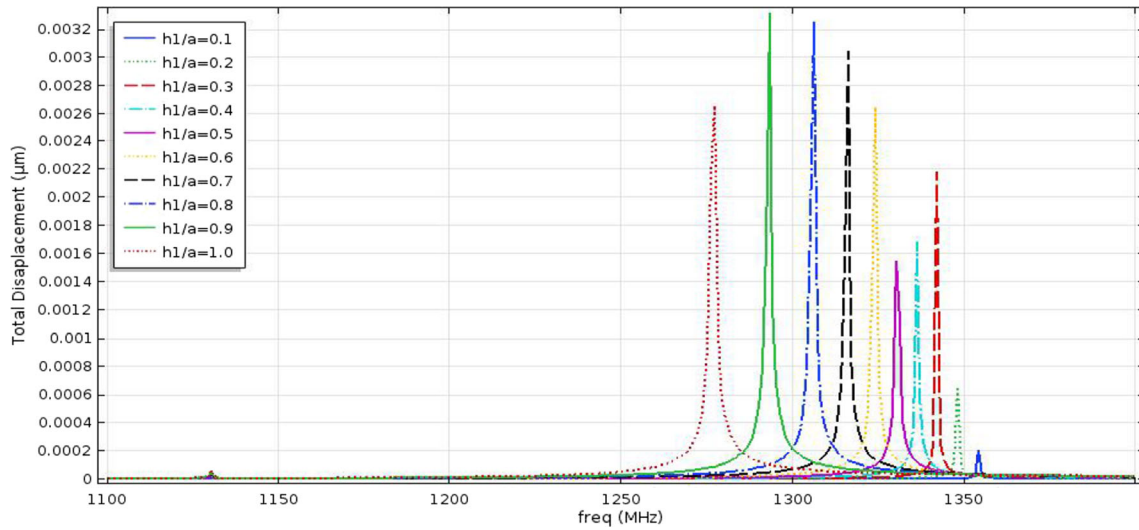| $h4/a$	0.1	0.2	0.3	0.4	0.5	0.6	0.7	0.8	0.9	1.0
f_a (MHz)	1355	1348	1342	1337	1331	1324	1316	1306	1293	1274
f_s (MHz)	1350	1343	1337	1332	1326	1319	1310	1300	1286	1266
k^2 (%)	0.910	0.915	0.919	0.922	0.927	0.932	1.125	1.134	1.336	1.549

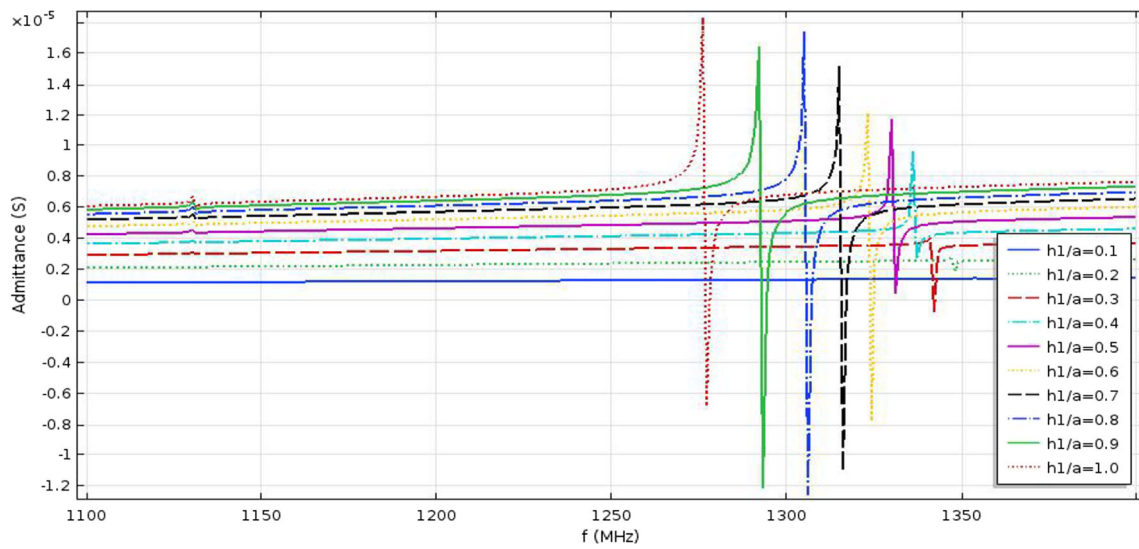Fig. 8 The influence of piezoelectric layer thickness on resonant displacement

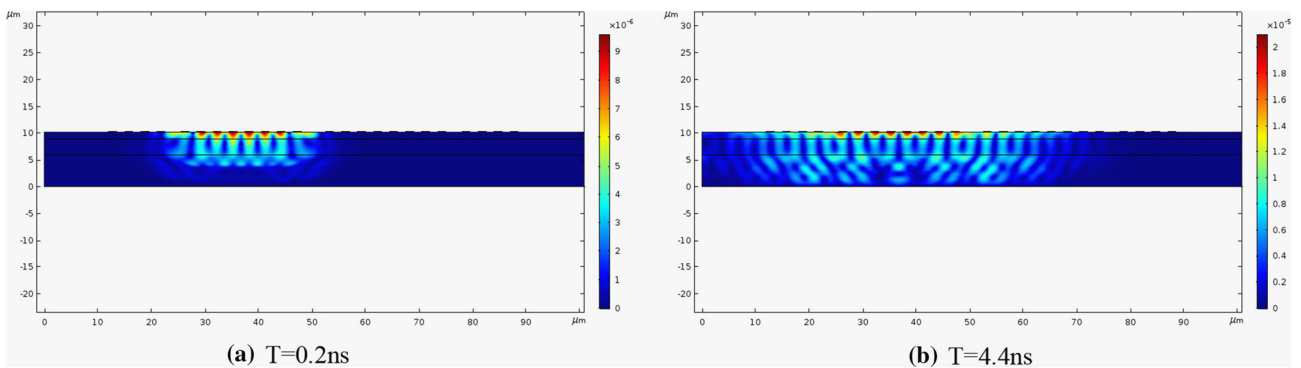Fig. 9 The influence of piezoelectric layer thickness on admittance

(a) T=0.2ns

(b) T=4.4ns

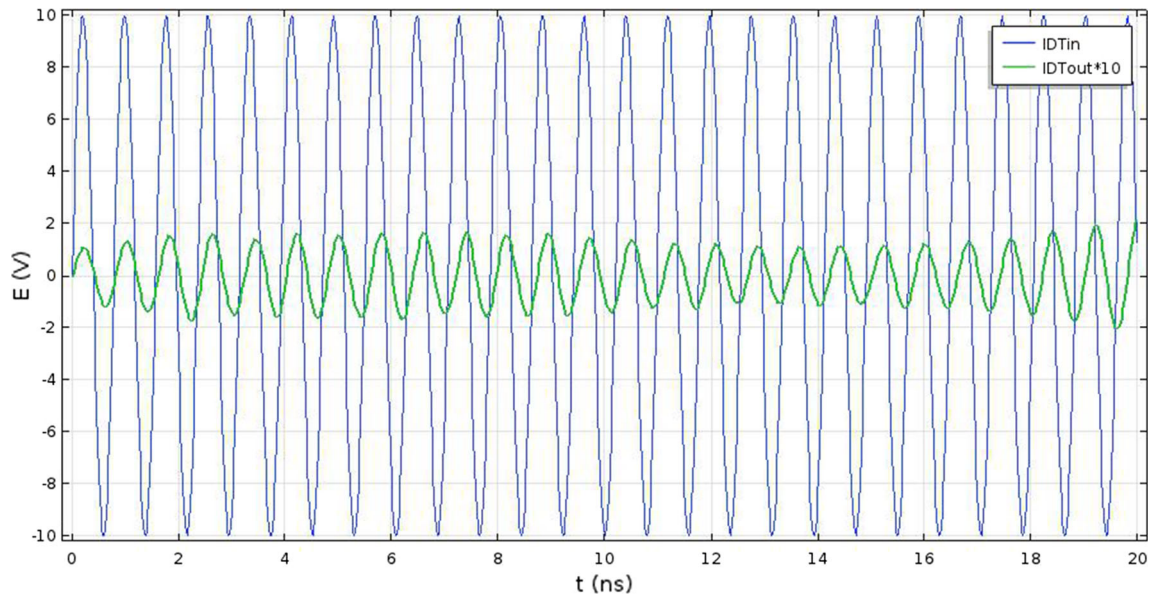Fig. 10 Propagation characteristics of SAWR

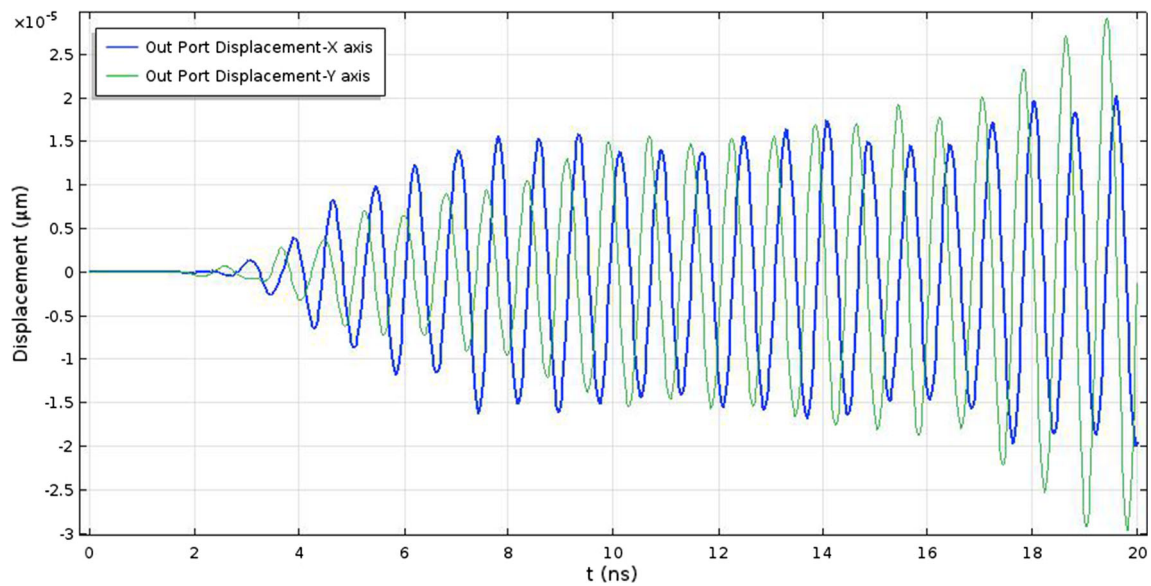**Fig. 11** Comparison of input and output voltages

Fig. 12 *X–Y* direction displacement comparison at output

thin film AlN are 0.78% (Tian et al. 2016). By comparing the resonant frequency and admittance characteristics, finally it can be concluded that the resonant state is the most significant when $h1/a = 1.0$.

Eventually, according to the design parameters optimized above, the complete 2D structure is modeled and analyzed in time domain. The transmission characteristics of SAWR, the comparison of input and output voltage signals and the analysis of output displacement are obtained.

From the transmission characteristics of Fig. 10, it can be seen that when the excitation is applied to the input, the piezoelectric layer generates surface waves and propagates

to both sides due to the mechanical change at the input end of the piezoelectric effect. At 4.4 ns, the mechanical deformation at the output end is obvious, and the output signal has a small time delay. The input voltage shown in Fig. 11 is $V = 10 * \sin(2\pi ft)V$, the applied time is 20 ns, and the signal frequency is 1270 MHz. According to the structure shown in Fig. 2, the output signal is obtained by transient analysis, but because of its small amplitude, the output value is ten times larger, and the peak value of the output is about 0.17 V.

According to Fig. 12, it can be seen that after 3 ns delay, the output end begins to vibrate obviously, and the

vibration amplitude of Y direction begins to exceed the amplitude of X direction at 14 ns and increases gradually. Within 3–20 ns, the variation of the amplitude of Y direction displacement and X direction displacement is the same, and always keeps a certain time delay.

6 Conclusion

In this paper, the 2D simulation of unit and complete AlN/diamond/Si layered structure is carried out. Through modal analysis, the designed two-port SAWR operating frequency is 1266.2 MHz. Then the enhancement of phase velocity and electromechanical coupling coefficient of the layered structure is realized by optimizing the design parameters. The optimal simulation results are obtained when the piezoelectric layer is $h1/a = 1.0$ and the electrode thickness is $h4/a = 0.1$. The phase velocity of the layered structure is 32.2% higher than that of the single AlN piezoelectric layer, and the electromechanical coupling coefficient also upgrade 49.6%. The time domain analysis of two-port SAWR obtains the comparison of input signal and output signal, analyses the actual wave propagation state, compares the vibration amplitudes of different directions, verifies the propagation mode of Rayleigh wave in work mode 1. Finally it lays a foundation for the actual production of GHz double-ended SAW resonator.

Author contributions All work with relation to this paper has been accomplished by all authors' efforts. The idea was proposed by LW. The simulation and its analysis were done by LW. HW gave significant guidance in the analysis.

Compliance with ethical standards

Conflict of interest The authors declare that there is no conflict of interest.

References

Adnan M, Franz D (2017) Surface acoustic wave (SAW) for chemical sensing applications of recognition layers. Sensors 17(12):2716

Aissa KA, Achour A, Elmazria O et al (2015) AlN films deposited by dc magnetron sputtering and high power impulse magnetron sputtering for SAW applications. J Phys D Appl Phys 48(14):145307

Aslam M, Jeoti V, Karuppanan S et al (2018) FEM analysis of Sezawa mode SAW sensor for VOC based on CMOS compatible AlN/SiO2/Si multilayer structure. Sensors 18(6):1687

Burkov SI, Zolotova OP, Sorokin BP et al (2018) Features of acoustic wave propagation in the Me/ZnO/Me/diamond waveguide structure. J Acoust Soc Am 143(1):16–22

Fu YQ, Luo JK, Nguyen NT, Walton AJ, Flewitt AJ, Zu XT, Li Y, McHale G, Matthews A, Iborra E, Du H, Milne WI (2017) Advances in piezoelectric thin films for acoustic biosensors, acoustofluidics and lab-on-chip applications. Prog Mater Sci 89:31–91

Fu S, Wang W, Qian L et al (2018) High frequency surface acoustic wave devices based on ZnO/SiC layered structure. IEEE Electron Device Lett 1:99

Fu C, Ke Y et al (2019) Investigation of rayleigh wave and love wave modes in 11$\bar{2}$0 ZnO film based multilayer structure. Surf Coat Technol 363(1):330–337

Hagelauer A, Fattinger G, Ruppel CCW, Ueda M, Hashimoto K, Tag A (2018) Microwave acoustic wave devices: recent advances on architectures, modeling, materials, and packaging. IEEE Trans Microw Theory Tech 66(10):4548–4562

Kaletta UC, Santos PV, Wolansky D et al (2013) Monolithic integrated SAW filter based on AlN for high-frequency applications. Semicond Sci Technol 28:065013. https://doi.org/10.1088/0268-1242/28/6/065013

Lirong Q (2009) Theoretical study on propagation characteristics of surface acoustic waves in multilayer structures. Tianjin University of Technology

Luo Jingting, Quan Aojie, Chen Fu, Li Honglang (2017) Shear-horizontal surface acoustic wave characteristics of a (110) ZnO/SiO2/Si multilayer structure. J Alloy Compd 693:558–564

Malik AF, Jeoti V, Fawzy M et al (2016) Estimation of SAW velocity and coupling coefficient in multilayered piezo-substrates AlN/SiO2/Si. In: 2016 6th international conference on intelligent and advanced systems (ICIAS). IEEE, Kuala Lumpur, Malaysia. https://doi.org/10.1109/ICIAS.2016.7824112

Maouhoub S, Aoura Y, Mir A (2016) FEM simulation of AlN thin layers on diamond substrates for high frequency SAW devices. Diam Relat Mater 62:7–13

Mortet V, Elmazria O, Nesladek M et al (2002) Surface acoustic wave propagation in aluminum nitride-unpolished freestanding diamond structures. Appl Phys Lett 81(9):1720

Mortet V, Williams OA, Haenen K (2008a) Diamond: a material for acoustic devices. Phys Status Solidi (a) 205(5):12

Mortet Vincent, Williams Oliver, Haenen K (2008b) Diamond: a material for acoustic devices. Phys Status Solidi (a) 205:1009–1020

Natalya F (2018) Multilayered structures using thin plates of LiTaO3 for acoustic wave resonators with high quality factor. Ultrasonics 88:115–122

Naumenko NF (2019) High-velocity non-attenuated acoustic waves in LiTaO3/quartz layered substrates for high frequency resonators. Ultrasonics 95:1–5

Nikolaou I, Hallil H, Tamarin O et al (2016) A three-dimensional model for a graphene guided SH- SAW sensor using finite element method. IEEE, Belo Horizonte, Brazil. https://doi.org/10.1109/SBMicro.2016.7731363

Ritter F, Hedrich J, Deck M et al (2017) Polymer structures on surface acoustic wave biosensors. Procedia Technol 27:35–36

Ro R, Chiang Y, Sung C, Lee R, Wu S (2010) Theoretical analysis of SAW propagation characteristics in (100) oriented AlN/diamond structure. IEEE Trans Ultrason Ferroelectr Freq Control 57(1):46–51

Ro R, Lee R, Lin ZX et al (2013) Surface acoustic wave characteristics of a (100) ZnO/(100) AlN/diamond structure. Thin Solid Films 529(2):470–474

Rodriguez-Madrid JG, Iriarte GF, Pedros J, Williams OA, Brink D, Calle F (2012) Super-high-frequency SAW resonators on AlN/diamond. IEEE Electron Device Lett 33(4):495–497

Ruppel CCW (2017) Acoustic wave filter technology: a review. IEEE Trans Ultrason Ferroelectr Freq Control 64(9):1390–1400

Sorokin AV, Shepeta AP (2017) Anti-collision radio-frequency identification system using passive SAW tags. In: Smart sensors, actuators, and MEMS VIII, vol 10246. International Society for Optics and Photonics, p 1024613. https://doi.org/10.1117/12.2263223

Sorokin BP, Kvashnin GM, Novoselov AS et al (2017) Excitation of hypersonic acoustic waves in diamond-based piezoelectric layered structure on the microwave frequencies up to 20 GHz. Ultrasonics 78:162

Tang IT, Chen HJ, Hwang WC et al (2004) Applications of piezoelectric ZnO film deposited on diamond-like carbon coated onto Si substrate under fabricated diamond SAW filter. J Cryst Growth 262(1–4):461–466

Tao W, Ryan G, Rajesh N et al (2015) Surface acoustic waves (SAW)-based biosensing for quantification of cell growth in 2D and 3D cultures. Sensors 15(12):32045–32055

Tian X, Tao L, Liu B, Zhou C, Yang Y, Ren T (2016) Surface acoustic wave devices based on high quality temperature-compensated substrates. IEEE Electron Device Lett 37(8):1063–1066

Vivek L, Nemade HB (2018) Finite element simulation of one-port surface acoustic wave resonator with thick interdigital transducer for gas sensing. Microsyst Technol 25:441. https://doi.org/10.1007/s00542-018-4015-y

Wang L, Chen S et al (2017) Enhanced performance of 17.7 GHz SAW devices based on AlN/diamond/Si layered structure with embedded nanotransducer. Appl Phys Lett 111(12):253502

Zhou J, Pang HF, Garcia-Gancedo L et al (2015) Discrete microfluidics based on aluminum nitride surface acoustic wave devices. Microfluid Nanofluid 18(4):537–548